
FUNGALZSL: ZERO-SHOT FUNGAL CLASSIFICATION WITH IMAGE CAPTIONING USING A SYNTHETIC DATA APPROACH

A PREPRINT

 **Anju Rani***
Department of Energy Technology
Aalborg University
Esbjerg, Denmark 6700
aran@energy.aau.dk

 **Daniel O. Arroyo**
Department of Energy Technology
Aalborg University
Esbjerg, Denmark 6700
doa@energy.aau.dk

 **Petar Durdevic**
Department of Energy Technology
Aalborg University
Esbjerg, Denmark 6700
pdl@energy.aau.dk

February 27, 2025

ABSTRACT

The effectiveness of zero-shot classification in large vision-language models (VLMs), such as Contrastive Language-Image Pre-training (CLIP), depends on access to extensive, well-aligned text-image datasets. In this work, we introduce two complementary data sources: one generated by large language models (LLMs) to describe the stages of fungal growth and another comprising a diverse set of synthetic fungi images. These datasets are designed to enhance CLIP’s zero-shot classification capabilities for fungi-related tasks. To ensure effective alignment between text and image data, we project them into CLIP’s shared representation space, focusing on different fungal growth stages. We generate text using LLaMA3.2 to bridge modality gaps and synthetically create fungi images. Furthermore, we investigate knowledge transfer by comparing text outputs from different LLM techniques to refine classification across growth stages.

An up-to-date repository accompanies this paper, including the dataset and resources discussed. [Synthetic Fungi Generation](#)

Keywords Deep learning · CLIP · Fungi · Synthetic dataset · Classification · Segmentation

1 Introduction

The emergence of large vision-language models (VLMs), such as CLIP (Contrastive Language-Image Pretraining) [Radford et al., 2021], BLIP (Bootstrapping Language-Image Pretraining) [Li et al., 2022], and ALIGN (A Large-scale Image and Noisy-text embedding) [Jia et al., 2021], represents a pivotal advancement in representation learning. These models leverage extensive datasets of image-text pairs to create shared embeddings that bridge the gap between visual and natural language domains [Min et al., 2023, Minaee et al., 2024, Mehta et al., 2024]. This bridging facilitates various downstream tasks, including zero-shot classification, where text descriptions are effectively matched to images. Despite their strengths, these models often encounter limitations in encoding detailed visual attributes within fine-grained domains, typically distinguishing categories at a high level. Additionally, the collection of large, domain-specific image-text datasets, particularly for specialized areas like fungi, presents significant resource challenges that complicate the training of these models.

*Use footnote for providing further information about author (webpage, alternative address)—*not* for acknowledging funding agencies.

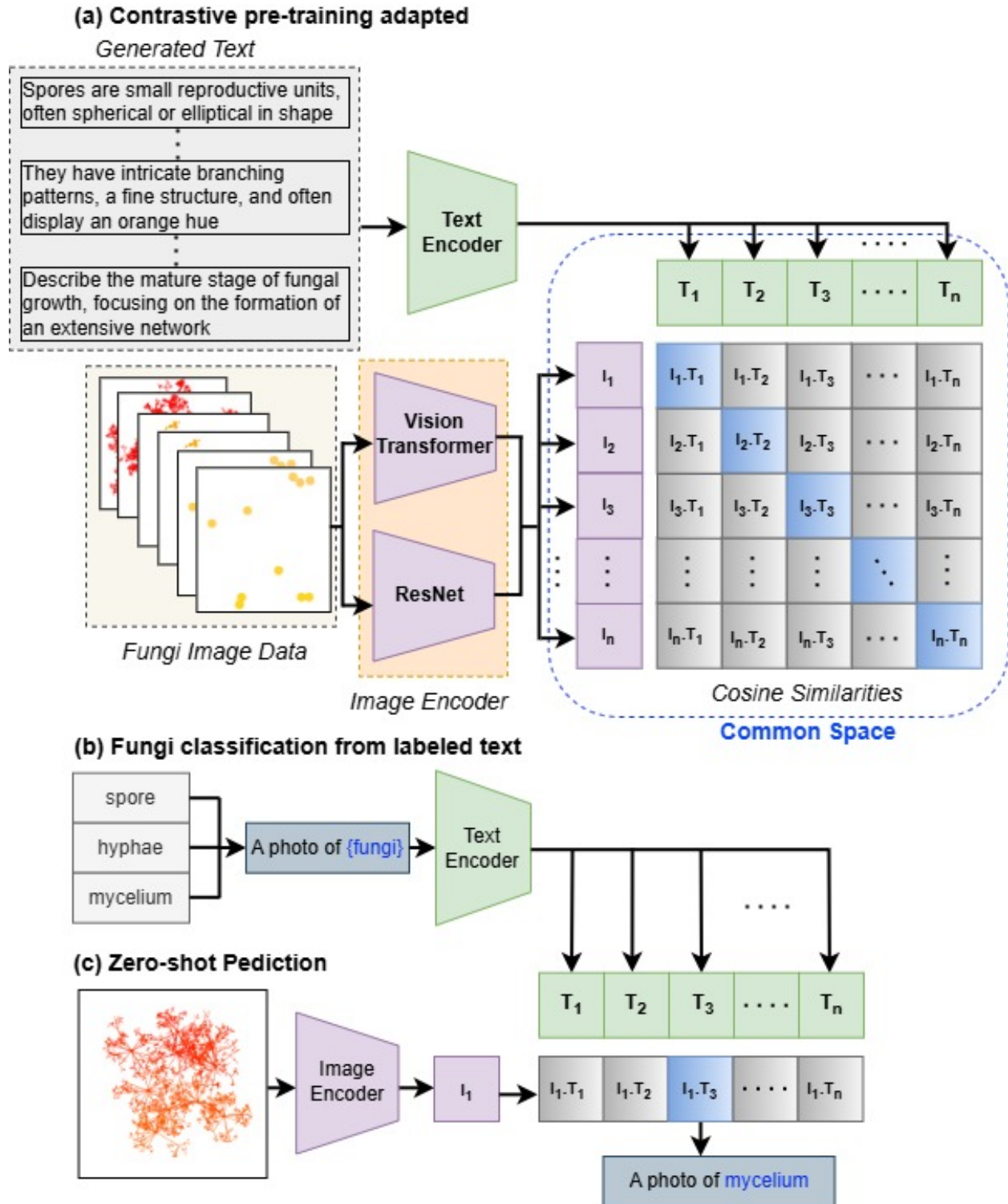


Figure 1: Overview of the adapted CLIP model.

VLMs such as CLIP [Radford et al., 2021] are designed to learn joint representations of images and text by training on large datasets of image-text pairs. By utilizing separate encoders for text and images, CLIP maps each modality into a shared embedding space where related pairs are positioned closely, while unrelated pairs are separated. This alignment is achieved using a contrastive loss (CL) function, which maximizes the similarity between correct image-text pairs

and minimizes it for mismatched pairs within each training batch. This framework enables CLIP to effectively manage large-scale, weakly supervised data and facilitates zero-shot learning, allowing it to classify images into unseen categories by matching them to textual prompts (e.g., “a photo of a [name of class]”). Consequently, CLIP is highly adaptable for transfer learning, with pre-trained encoders that can quickly adjust to new tasks with minimal additional data. The BLIP model [Li et al., 2022] enhances vision-language pretraining through a bootstrapping approach that generates high-quality image-text pairs. It consists of two key components: Bootstrapped Data Generation, which generates relevant captions for images to iteratively refine the dataset for improved semantic alignment, and a contrastive learning (CL) objective that aligns embeddings of related image-text pairs while distancing unrelated ones, paralleling the methods used in CLIP and ALIGN. BLIP has demonstrated strong performance in zero-shot image classification, visual question answering, and image-text retrieval, achieving high accuracy by filtering training data effectively and minimizing dependence on noisy web sources. The ALIGN model [Jia et al., 2021] capitalizes on vast noisy image-text pairs derived from alt-text annotations on the web. By employing a CL framework, ALIGN achieves robust zero-shot and transfer learning capabilities across diverse tasks without requiring extensive fine-tuning (FT). Its approach effectively navigates the noise inherent in web-based data, leveraging its sheer volume to enhance learning outcomes.

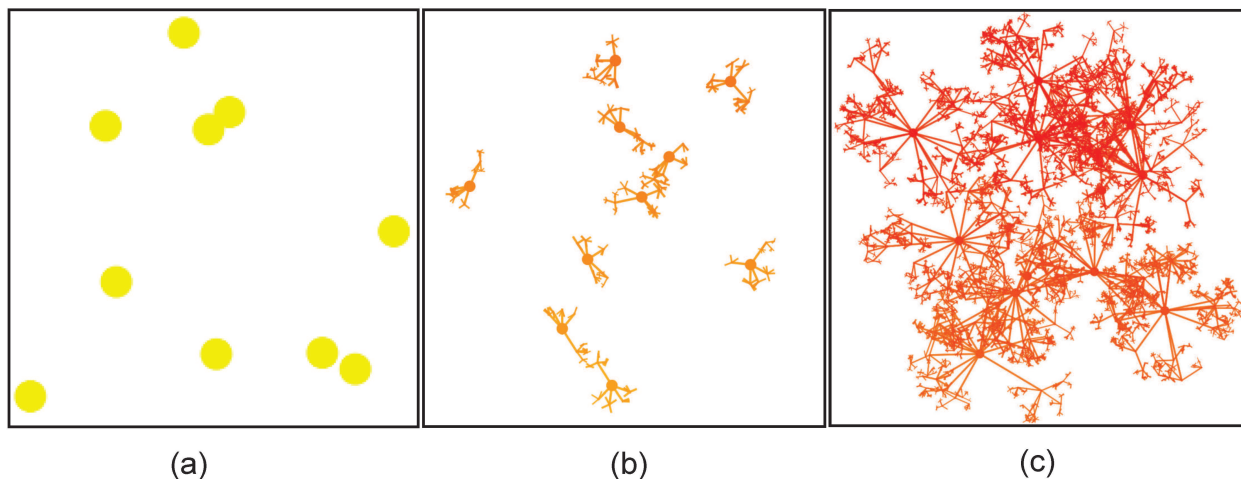
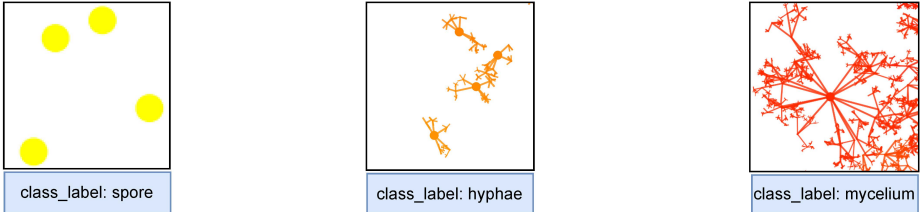


Figure 2: Fungi Dataset: (a) Spore, (b) Hyphae, and (c) Mycelium.

Moreover, the classification with Hierarchical Label Sets (CHiLS) framework [Novack et al., 2023] significantly enhances zero-shot image classification performance for models like CLIP by incorporating a hierarchical structure into class labels. This methodology improves model accuracy by substituting coarse class labels with fine-grained subclasses that better reflect semantic relationships, resulting in notable performance gains—up to 30 % higher accuracy in datasets with inherent hierarchical structures. CHiLS maintains consistent improvements even in the absence of explicit hierarchical data by generating approximate subclasses through prompts to GPT-3. This adaptable approach requires no additional training costs and can be seamlessly integrated into existing zero-shot classification pipelines. Recently, the CatLIP model [Mehta et al., 2024] has introduced an innovative shift in vision model pre-training by framing the task on image-text data as a classification problem rather than utilizing CLIP’s CL approach. This transformation eliminates the need for pairwise similarity calculations, resulting in a 2.7x acceleration in training on large-scale datasets compared to CLIP. Furthermore, CatLIP enhances data-efficient transfer learning by employing its classification layer to initialize classifiers for target tasks. Unlike CLIP, CatLIP exhibits improved performance with extended training on smaller datasets, successfully avoiding early saturation in performance.

The evolution of **large language models (LLMs)** has been marked by significant advancements, starting with GPT [Radford et al., 2018], which introduced the transformer architecture for unsupervised learning on large text data. GPT-2 [Radford et al., 2019] scaled up the model to 1.5 billion parameters, showcasing its ability to generate coherent text and perform various tasks without FT, while raising ethical concerns about potential misuse. Building on this, GPT-3 [Radford et al., 2021] further increased the parameter count to 175 billion, demonstrating remarkable capabilities in zero-shot and few-shot learning. The subsequent GPT-4 [OpenAI, 2023] improved reasoning and contextual understanding, solidifying its reliability for diverse applications. The Mistral model [Jiang et al., 2023], designed specifically for efficiency and performance, contributes to the field by delivering high-quality outputs while focusing on reducing computational costs, making it an attractive option for resource-constrained environments. Additionally, models like Gemini [Team et al., 2023] and Claude [Bai et al., 2022] have pushed the boundaries of multimodal reasoning and safety, enhancing AI alignment and interoperability. Meanwhile, LLaMA [Touvron et al., 2023] introduced a



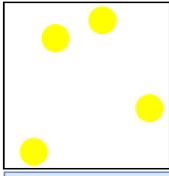
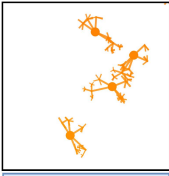
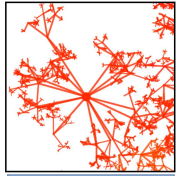
| | | | |
|---|---|--|---|
| |  class_label: spore |  class_label: hyphae |  class_label: mycelium |
| GPT-4o1 | These yellow circles might be interpreted as discrete "spots" or colonies on a simple background, akin to individual microbial colonies growing on a plate, or droplets of fluorescently labeled cells in a microfluidic experiment. | These individual orange shapes resemble simplified schematic representations of branching cells or organisms. Each structure has a roughly spherical "body" or "cell," with multiple "arms" radiating outward. The arms then branch or terminate in smaller nodules, much like dendrites on a neuron, the hyphal tips of fungi, or the branching extremities of certain colonial microorganisms. | It is a highly branched network reminiscent of certain natural growth or branching processes. Each large circular "node" could be interpreted as a major branching point—similar to a hub in a mycelial (fungal) network, a branching point in a neuron's dendritic tree, or a node in a radial phylogenetic diagram. |
| LlaMa 3.2 | Describe the early stage of fungal growth, focusing on spore formation. Spores are small reproductive units, often spherical or elliptical in shape, produced in large quantities to disperse and initiate fungal growth in new areas. Fungi reproduce sexually and asexually, with spores being the primary means of asexual reproduction. | Describe the development of fungal hyphae. Hyphae are thread-like, elongated filaments that spread and branch, forming a complex network to absorb nutrients. Focus on the expansion and structure of hyphae. The development of fungal hyphae is a complex process that involves the coordinated growth and branching of thread-like filaments. | Describe the mature stage of fungal growth, focusing on the formation of an extensive mycelium network. The mycelium is made up of interwoven hyphae, forming a dense structure that absorbs nutrients. Describe the types of fungi that exhibit this mature stage of growth. Explain the importance of the mycelium network in the life cycle of fungi. The mature stage of fungal growth. |
| Gemini 2.0 | In a biological context, this could represent individual cells in a culture, organisms in a population, or even the distribution of specific molecules. The focus moves away from interaction and towards the properties and arrangement of independent units. | The presence of multiple distinct, branching clusters with limited interconnections points towards a different set of biological phenomena. This could represent isolated communities of cells, separate organ systems with limited interaction, or fragmented ecosystems. | The hierarchical branching and central origin strongly suggest processes like neural networks, vascular systems, or root growth, where distribution and connectivity from a central source are paramount. |
| Claude 3.5 | Image depicts what appears to be a cell distribution analysis, possibly representing cell bodies or nuclei (shown as yellow circles) in a defined field of view. | Image shows what appears to be individual neurons in their early developmental stage or in a sparse culture. The orange-coloured structures display characteristic neuronal morphology with cell bodies represented by circular nodes and extending processes shown as branching lines. | A dendritic network pattern exhibits hierarchical branching from central nodes, which is characteristic of biological structures like neural networks or fungal mycelia. The image represents a much more complex and mature neuronal network. |
| Text Prompt : Assume yourself as a bio-scientist, explain the image. | | | |

Figure 3: Textual description of using various LLMs.

family of models optimized for research, ranging from 7 billion to 70 billion parameters, aiming to democratize access to large models while maintaining competitive performance. Building upon these advancements, OpenAI introduced GPT-4o1, a model that emphasizes "thinking" before responding, thereby enhancing its problem-solving capabilities in complex domains such as science, coding, and mathematics. Together, these models illustrate the rapid progress in natural language processing (NLP) and their expanding utility across various domains. While much of the prior research has concentrated on refining text descriptions for a wide array of generic classes, the ongoing exploration of LLMs-specific applications and adaptations continues to expand their utility. This focus not only enhances the performance of these models in general tasks but also paves the way for tailored approaches that address more specialized domains and complex user needs. To address the limitations of existing models in recognizing fine-grained categories, particularly in the context of fungi growth stages, we propose a novel VLM framework. This work leverages two primary data sources—LLMs and extensive synthetic fungi image datasets—to enhance zero-shot classification performance across these fine-grained domains. Specifically, we generate a synthetic fungi dataset and align it with text descriptions produced by LLMs for each class label, capturing various stages of fungi growth. This approach is effective because the fungi image dataset is fine-grained, unlike broader categories with high-class variation. Additionally, the synthetic fungi dataset uses LLMs to generate scalable descriptions of essential features, such as shape, color, branching, and growth stage. The use of fine-grained labels aids in bridging the gap between closely related images of fungi growth stages, which is crucial for training large VLMs. Figure 1 illustrates the adapted approach used in this study.

The contributions of this paper are summarized as follows:

1. A novel synthetic image dataset was generated to represent different fungal growth stages capturing fine-grained structural variations.
2. Various LLMs (LLaMA 3.2, GPT-4o1, Claude 3.5, and Gemini 2.0) were used to generate and compare textual descriptions of fungal growth stages.
3. Systematic FT to improve CLIP performance by bridging the modality gap between synthetic images and text descriptions.
4. Comprehensive evaluation using quantitative metrics, and visual inspections.

The paper is structured as follows: Section 2 outlines the methodology used in this work, detailing the process of generating a synthetic fungi dataset and its corresponding textual descriptions. Section 3 presents the implementation details and the results obtained from our experiments. Finally, Section 4 offers concluding remarks, summarizing our findings and discussing their implications.

2 Methodology

We pre-train LLMs on paired multi-modal data to enable multi-modal understanding, specifically focusing on image and text narrations. This process involves training an encoder that projects input data into the text token embedding space of a designated LLM, effectively transforming the LLM’s text token embedding space into a joint token embedding space for enhanced interaction between modalities.

The proposed method is evaluated through zero-shot classification on novel fungi classes by assessing the ability of CLIP to recognize fungal growth stages based on textual descriptions generated by different LLMs. To enhance the effectiveness of large VLMs, we generate detailed class descriptions for spore, hyphae, and mycelium using LLaMA 3.2 and test their impact on classification when replaced with descriptions from other LLMs, including GPT-4o1, Claude 3.5, and Gemini 2.0. We employ diverse prompting techniques to improve text-image alignment and assess how well the model generalizes across different textual representations. A summary of the consistent improvements in text generation across LLMs is presented in Figure 2.

2.1 Generation of Fungi Dataset

Consider a dataset with three classes Class 1: spore (early-stage), Class 2: hyphae (mid-stage), and Class 3: mycelium (mature-stage). Each class has its unique structure and is represented by different characteristics (number of spores, branch structures, given by:

$$C = (C_s, C_h, C_m) \quad (1)$$

where C_s , C_h , and C_m are the three classes of fungi dataset spore, hyphae and mycelium respectively. For each class C_k , where $k \in (\text{spore, hyphae, mycelium})$, we define the parameters: N_k : number of structures, D_k : depth of branching, L_k : length of branches, and W_k : width of branches. These parameters control the structure’s appearance in each stage. For each class C_k , define a function $G_k(x, y; \theta_k)$ that generates the structures at random positions (x, y) with the parameter vector $\theta_k = (N_k, D_k, L_k, W_k)$.

1. *Spore Class Generation*: Define $G_s(x, y; N_s)$ as a set of circular points F centered at (x, y) with radius r representing the spores:

$$G_s(x, y; N_s) = \sum_{i=1}^{N_s} F((x_i, y_i), r) \quad (2)$$

2. *Hyphae Class Generation*: Define $G_h(x, y; \theta_h)$ as a central spore with branching lines extending outward, where $\theta_h = (N_h, D_h, L_h, W_h)$. For each spore centre (x_i, y_i) , draw branches with recursive depth D_h and initial branch length L_h :

$$G_h(x, y; \theta_h) = \sum_{i=1}^{N_h} [F((x_i, y_i), r) + \sum_{d=1}^{D_h} B(L_h \cdot \alpha^d, W_h \cdot \beta^d)] \quad (3)$$

3. *Mycelium Class Generation*: Define $G_m(x, y; \theta_m)$ with the most complex branching pattern, where $\theta_m = (N_m, D_m, L_m, W_m)$.

$$G_m(x, y; \theta_m) = \sum_{i=1}^{N_m} [F((x_i, y_i), r)] + \sum_{d=1}^{D_m} B(L_m \cdot \alpha^d, W_m \cdot \beta^d) \quad (4)$$

Finally, to generate the dataset (D_{final}), we iterate over all the classes C_k and generate images for each class:

$$D_{final} = \sum_{k \in (s, h, m)} \sum_{i=1}^{N_k} [F((x_i, y_i), r)] + \sum_{d=1}^{D_k} B(L_k \cdot \alpha^d, W_k \cdot \beta^d) \quad (5)$$

Consider a dataset $D_{final} = \{(q_i, r_i) \mid i = 1, \dots, N\}$, where $q_i \in X$ represents images and $r_i \in Y$ represents corresponding text descriptions. Large VLMs like CLIP use an image encoder (I) and a text encoder (T) such that $I(q) \approx T(r)$ when an image q matches a text description r . In this work, we fine-tune CLIP using a synthetically generated fungi dataset, where the text descriptions are produced by LLMs. The dataset is divided into training, validation, and test sets, encompassing three distinct class labels—*spore*, *hyphae*, and *mycelium*—which correspond to different stages of the fungal life cycle. The generated synthetic fungi dataset is open-source and available at [Rani et al., 2025a].

The generated fungi dataset is designed to realistically represent each growth stage by incorporating subtle overlaps between stages and unique color gradients for each type. To capture the natural progression of growth, each stage includes traces of the previous one [Rani et al., 2025b]. For instance, hyphae images contain a few spores, suggesting that not all cells have fully transitioned to hyphae. Similarly, mycelium images reflect the incomplete transition to mature mycelium by including some hyphae. The specific color gradients used for each fungi stage are as follows:

1. Spore: Features a gradient from bright yellow to orange, symbolizing the earliest growth phase.
2. Hyphae: Progresses from orange to a deeper orange, indicating further development.
3. Mycelium: Shifts from red-orange to deep red, representing a mature growth phase.

The image generation is structured over a 100 s timeline, with each stage represented by a specific temperature range.

1. Spore Generation: This phase maps temperatures from 300 K to 330 K, covering the initial formation of spores.
2. Hyphae Growth: The temperature increases from 330 K to 370 K, aligning with the development of hyphae.
3. Mycelium Formation: Temperatures rise from 370 K to 400 K, culminating in the mature mycelium stage.

This structured approach provides realistic progression across stages, with carefully selected colors and temperature mappings to enhance the visual and temporal differentiation of each growth phase [Rani et al., 2025a]. Figure 2 illustrates an example of the generated fungi dataset.

The proposed model is evaluated on unseen fungi classes by calculating the similarity score, where for any image q with a textual description r , the similarity score $S(q, r)$ is computed as the cosine similarity between the image encoder’s output $I(q)$ and the text encoder’s output $T(r)$.

2.2 Generation of Textual Description

The textual descriptions for each class are generated based on prompts tailored to the specific fungal growth stage, emphasizing attributes such as color, structure, development, and function. Here, $[class]$ represents the class label for each of the k classes in the fungi dataset: spore, hyphae, and mycelium. The LLM generates r_k textual descriptions for each class k , ensuring diversity and relevance through probabilistic sampling techniques. Prompts such as “Describe the fungal growth stage $[class]$, focusing on its key biological characteristics,” guide the model to produce detailed descriptions. These descriptions take the form of contextual explanations, such as “ $[class]$ characterized by $[characteristics]$,” resulting in a set of descriptions r^k for each class k . The impact of these characteristic-based descriptions has led to notable improvements, as shown in Figure 3.

The class-level textual descriptions used in training were generated utilizing LLaMA 3.2 and then validated with various other APIs: (a) GPT-4o1, (b) Gemini 2.0, and (c) Claude 3.5. We set the temperature parameter to 0.9, allowing the models to incorporate more randomness and produce diverse textual descriptions for each image class across the dataset. For each class C , descriptions are generated using predefined prompts. Each caption satisfies constraints on

length L , with $L_{min} \leq L \leq L_{max}$. For N descriptions with batch size B , the captions are generated over $\lceil N/B \rceil$ batches, given by:

$$r(C, N) = \bigcup_{k=1}^{\lceil N/B \rceil} r_k(C, B) \quad (6)$$

where $r_k(C, B)$ is the set of captions in the k -th batch.

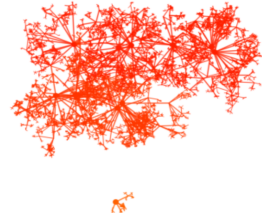
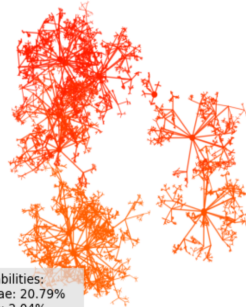
| | |
|---|--|
| <p>Image Index: 171</p> <p>Original description: These individual orange shapes resemble simplified schematic representations of branching cells or organisms. Each structure has a roughly spherical body or cell, with multiple arms radiating outward. The arms then branch or terminate in smaller nodules, much like dendrites on a neuron, the hyphal tips of fungi, or the branching extremities of certain colonial microorganisms.</p> <p>Predicted class: hyphae</p>  <p>Probabilities: hyphae: 83.63% spore: 8.35% mycelium: 8.02%</p> | <p>Image Index: 164</p> <p>Original description: These individual orange shapes resemble simplified schematic representations of branching cells or organisms. Each structure has a roughly spherical body or cell, with multiple arms radiating outward. The arms then branch or terminate in smaller nodules, much like dendrites on a neuron, the hyphal tips of fungi, or the branching extremities of certain colonial microorganisms.</p> <p>Predicted class: hyphae</p>  <p>Probabilities: hyphae: 89.81% spore: 3.56% mycelium: 6.63%</p> |
| <p>Image Index: 48</p> <p>Original description: These yellow circles could be interpreted as isolated spherical structures (e.g., spores, single celled organisms, or microcolonies) on a plain background. The variation in yellow hue may indicate slight differences in density, maturity, or metabolic state. Their scattered distribution—with no visible connections or branching—suggests they are independent units, rather than part of an organized network. This arrangement might be seen in a low density cell culture or a sparse spread of spores on an agar plate, where each circle represents a discrete biological entity.</p> <p>Predicted class: spore</p>  <p>Probabilities: hyphae: 16.96% spore: 70.31% mycelium: 12.73%</p> | <p>Image Index: 217</p> <p>Original description: It is a highly branched network reminiscent of certain natural growth or branching processes. Each large circular "node" could be interpreted as a major branching point—similar to a hub in a mycelial (fungal) network, a branching point in a neuron's dendritic tree, or a node in a radial phylogenetic diagram.</p> <p>Predicted class: mycelium</p>  <p>Probabilities: hyphae: 16.11% spore: 1.84% mycelium: 82.06%</p> |
| <p>Image Index: 292</p> <p>Original description: It is a highly branched network reminiscent of certain natural growth or branching processes. Each large circular "node" could be interpreted as a major branching point—similar to a hub in a mycelial (fungal) network, a branching point in a neuron's dendritic tree, or a node in a radial phylogenetic diagram.</p> <p>Predicted class: mycelium</p>  <p>Probabilities: hyphae: 20.79% spore: 2.04% mycelium: 77.17%</p> | <p>Image Index: 80</p> <p>Original description: These yellow circles could be interpreted as isolated spherical structures (e.g., spores, single celled organisms, or microcolonies) on a plain background. The variation in yellow hue may indicate slight differences in density, maturity, or metabolic state. Their scattered distribution—with no visible connections or branching—suggests they are independent units, rather than part of an organized network. This arrangement might be seen in a low density cell culture or a sparse spread of spores on an agar plate, where each circle represents a discrete biological entity.</p> <p>Predicted class: spore</p>  <p>Probabilities: hyphae: 17.74% spore: 70.92% mycelium: 11.34%</p> |

Figure 4: Zero-shot classification with proposed CLIP model: (a) top: GPT-4o1, (b) centre: Claude 3.5, and (c) bottom: Gemini 2.0

2.3 CLIP Fine-tuning

Fine-tuning encompasses a range of techniques aimed at adjusting the parameters of a pre-trained model to optimize its performance on specific downstream tasks. As mentioned in Section 2, for q^k set of images we have r^k set of texts for $k \in D_{final}$ in the fungi training set. In this work, fine-tuning is performed by continuing CL with image-text pairs. We initialize CLIP’s model (RN50, ViT-B/32, ViT-B/16, and ViT-L/14@336px) and optimize the contrastive loss. The loss function for image and text is given by:

$$L_{image} = -\frac{1}{N} \sum_{q=1}^N \frac{1}{|P_q|} \sum_{r \in P_q} \log \frac{e^{S_{q,r}/\tau}}{\sum_{r=1}^N e^{S_{q,r}/\tau}} \quad (7)$$

and

$$L_{text} = -\frac{1}{N} \sum_{r=1}^N \frac{1}{|P_r|} \sum_{q \in P_r} \log \frac{e^{S_{q,r}/\tau}}{\sum_{r=1}^N e^{S_{q,r}/\tau}} \quad (8)$$

where τ represent learnable temperature parameter, $S_{q,r}$ represents the correct similarity metric (e.g., cosine similarity) between image q and text r , P_q represents the set of positive text matches for image q while and P_r represents the set of positive image matches for text r . The final contrastive loss (CL) is given by:

$$L_{total} = L_{image} + L_{text} \quad (9)$$

Table 1: Recall@1 qualitative results.

| CLIP Model | Learning rate | Iteration rate | Value |
|----------------|---------------|----------------|--------------|
| RN50 | 1e-6 | 2.32 s/it | 0.333 |
| ViT-B/16 | 1e-6 | 15.95 s/it | 0.913 |
| ViT-B/32 | 1e-6 | 15.50 s/it | 0.670 |
| ViT-L/14@336px | 1e-6 | 3.86 s/it | 0.973 |

3 Results and Discussion

This section assesses the proposed method against baseline models under various settings. The evaluation focuses on the synthetic fungal dataset introduced in Section 2.1, tested across different architectures. The approach effectively scales across architectures with few training epochs.

Model Performance: The proposed model was fine-tuned using a batch size of 512 on an NVIDIA GeForce RTX 4090. The fine-tuned CLIP model was trained on a dataset comprising fungal images and LLM-generated textual descriptions, aiming to distinguish key biological structures. The synthetic fungal dataset used in this study consisted of 6,000 images, split into 4,800 for training, 600 for testing, and 600 for validation, and was trained for 100 epochs. The fine-tuning (FT) strategy of pairing image-text samples within classes provides a streamlined and efficient approach for zero-shot fungal classification.

Initially, CLIP’s parameters were frozen to preserve its broad representations from large-scale pretraining. Transformer layers were incrementally unfrozen every five epochs, enabling a progressive FT process. This stepwise unfreezing allowed the model to adapt to the synthetic fungal dataset while maintaining stable learning. Layers were unfrozen in reverse order, starting from the last transformer block, ensuring that lower-level transferable features remained intact. This approach led to better convergence while optimizing computational efficiency, making the FT process feasible even with limited resources. The AdamW optimizer was applied exclusively to the unfrozen layers, ensuring efficient parameter updates.

Inference on the validation set produced promising classification results, with the model assigning high-confidence predictions to the correct labels in most cases. The probability distribution of predictions revealed that the model effectively differentiated between hyphae, spores, and mycelium with reasonable certainty. However, some misclassifications were observed, likely due to overlapping visual features among specific categories. Figures 4 illustrate the zero-shot classification performance of the fine-tuned CLIP model when paired with textual descriptions from different LLMs: GPT-4o1, Claude 3.5, and Gemini 2.0. The CLIP model demonstrated strong recognition capabilities for fungal growth stages across various LLM-generated descriptions. High similarity scores between text and image

embeddings indicate that these prompts effectively capture fungal structural characteristics. However, descriptions from Claude 3.5, while informative, were less aligned with the synthetic fungal dataset. Furthermore, Gemini 2.0 exhibited the lowest classification accuracy, suggesting its textual outputs lacked the specificity required for optimal alignment.

These findings emphasize the importance of well-structured, domain-specific textual descriptions in bridging the modality gap. The results further indicate that text quality significantly influences classification accuracy, with GPT-generated captions yielding the most precise alignments. This suggests that incorporating high-quality, domain-specific textual representations can enhance fungi classification performance.



Figure 5: Recall@1 qualitative results. The predicted and true class labels from the validation dataset have been mentioned in this figure. The results which are correctly ranked as 1 for their corresponding class label are bordered green while incorrect results have been bordered red.

Performance Across Architectures: Table 1 presents the classification performance of different CLIP model architectures trained on the synthetic fungal dataset:

- ViT-L/14@336px: These architectures achieved the highest Recall@1 score of 0.97, indicating high performance in fungal image-text alignment. The results suggest that increasing model complexity leads to significant accuracy gains for the fungi dataset.
- ViT-B/32 and ViT-B/16: This model demonstrated a Recall@1 score of 0.67 and 0.91, respectively.
- RN50: This model exhibited the lowest Recall@1 score (0.333), indicating that convolution-based architectures may be less effective in capturing fine-grained fungal features.

These results confirm that transformer-based architectures, particularly ViT-based CLIP variants, are better suited for zero-shot fungal classification tasks.

Error Analysis: Figure 5 visualizes the predicted class labels from the validation dataset, providing insight into the model’s classification behavior. The model exhibited high confidence in correctly classifying spores and hyphae. However, misclassifications were observed between hyphae and mycelium due to their overlapping structural characteristics. Lower confidence scores were recorded for ambiguous samples, highlighting areas where text-image alignment could be further refined, as discussed in Figures 4.

Overall, the results indicate that ViT-L/14@336px achieved the best classification accuracy, demonstrating strong alignment with the synthetic fungal dataset. The effectiveness of textual descriptions was evident, with GPT-4o1 outperforming Claude 3.5 and Gemini 2.0 in generating highly relevant prompts that enhanced classification performance. Misclassifications primarily occurred in visually similar growth stages, suggesting that refining text-image alignment could further improve accuracy. These findings highlight the potential of integrating synthetic datasets with LLM-generated text to advance zero-shot fungal classification.

4 Conclusion and Future Work

This study demonstrates the effectiveness of enhancing zero-shot classification in vision-language models (VLMs) like CLIP by integrating synthetic fungal images and LLM-generated textual descriptions. By aligning these complementary datasets within CLIP’s shared representation space, we successfully improved classification performance across different fungal growth stages. Fine-tuning CLIP with domain-specific synthetic data enhanced generalization and minimized modality gaps, while the inclusion of diverse LLM-generated text significantly refined classification accuracy. Additionally, transformer-based architectures, particularly ViT-L/14@336px, exhibited superior performance compared to convolution-based models like RN50, confirming their suitability for fine-grained fungal classification.

Despite these advancements, several areas remain for future improvement. Expanding the dataset to include additional fungal growth stages and diverse environmental conditions could improve model generalization. Enhanced text representations, such as richer text embeddings or multi-label classification, may help mitigate ambiguities in class descriptions, particularly in visually similar categories like hyphae and mycelium. Moreover, FT with domain-specific loss functions, such as contrastive learning tailored for biological classification, could further strengthen the semantic alignment between image and text embeddings. Another promising direction is refining the model’s robustness against classification errors by improving text-image alignment strategies and leveraging more structured textual prompts. Additionally, the progressive fine-tuning approach used in this study, where transformer layers were gradually unfrozen, proved effective in optimizing computational efficiency while maintaining stable learning. Future work could explore adaptive fine-tuning strategies that dynamically adjust layer unfreezing based on validation performance, further reducing computational overhead while enhancing model adaptation.

Overall, this research contributes to advancing automated fungal identification, with potential applications in microbiological monitoring studies. Future refinements in dataset diversity, hierarchical label structures, and optimization strategies could further strengthen zero-shot classification capabilities in specialized biological domains.

Ethics Statement

This research does not involve experiments, observations, or data collection related to human or animal subjects.

Declaration of competing interest

The authors declare that they have no known competing financial interests or personal relationships that could have appeared to influence the work reported in this paper.

Data Availability

[Synthetic Fungi Generation.](#)

References

- Alec Radford, Jong Wook Kim, Chris Hallacy, Aditya Ramesh, Gabriel Goh, Sandhini Agarwal, Girish Sastry, Amanda Askell, Pamela Mishkin, Jack Clark, et al. Learning transferable visual models from natural language supervision. In *International conference on machine learning*, pages 8748–8763. PMLR, 2021.
- Junnan Li, Dongxu Li, Caiming Xiong, and Steven Hoi. Blip: Bootstrapping language-image pre-training for unified vision-language understanding and generation. In *International conference on machine learning*, pages 12888–12900. PMLR, 2022.
- Chao Jia, Yinfei Yang, Ye Xia, Yi-Ting Chen, Zarana Parekh, Hieu Pham, Quoc Le, Yun-Hsuan Sung, Zhen Li, and Tom Duerig. Scaling up visual and vision-language representation learning with noisy text supervision. In *International conference on machine learning*, pages 4904–4916. PMLR, 2021.
- Bonan Min, Hayley Ross, Elior Sulem, Amir Pouran Ben Veyseh, Thien Huu Nguyen, Oscar Sainz, Eneko Agirre, Ilana Heintz, and Dan Roth. Recent advances in natural language processing via large pre-trained language models: A survey. *ACM Computing Surveys*, 56(2):1–40, 2023.
- Shervin Minaee, Tomas Mikolov, Narjes Nikzad, Meysam Chenaghlu, Richard Socher, Xavier Amatriain, and Jianfeng Gao. Large language models: A survey. *arXiv preprint arXiv:2402.06196*, 2024.
- Sachin Mehta, Maxwell Horton, Fartash Faghri, Mohammad Hossein Sekhavat, Mahyar Najibi, Mehrdad Farajtabar, Oncel Tuzel, and Mohammad Rastegari. Catlip: Clip-level visual recognition accuracy with 2.7 x faster pre-training on web-scale image-text data. *arXiv preprint arXiv:2404.15653*, 2024.
- Zachary Novack, Julian McAuley, Zachary Chase Lipton, and Saurabh Garg. Chils: Zero-shot image classification with hierarchical label sets. In *International Conference on Machine Learning*, pages 26342–26362. PMLR, 2023.
- Alec Radford, Karthik Narasimhan, Tim Salimans, Ilya Sutskever, et al. Improving language understanding by generative pre-training. 2018.
- Alec Radford, Jeffrey Wu, Rewon Child, David Luan, Dario Amodei, Ilya Sutskever, et al. Language models are unsupervised multitask learners. *OpenAI blog*, 1(8):9, 2019.
- OpenAI. Gpt-4 technical report. arxiv 2303.08774. *View in Article*, 2(5), 2023.
- Albert Q Jiang, Alexandre Sablayrolles, Arthur Mensch, Chris Bamford, Devendra Singh Chaplot, Diego de las Casas, Florian Bressand, Gianna Lengyel, Guillaume Lample, Lucile Saulnier, et al. Mistral 7b. *arXiv preprint arXiv:2310.06825*, 2023.
- Gemini Team, Rohan Anil, Sebastian Borgeaud, Jean-Baptiste Alayrac, Jiahui Yu, Radu Soricut, Johan Schalkwyk, Andrew M Dai, Anja Hauth, Katie Millican, et al. Gemini: a family of highly capable multimodal models. *arXiv preprint arXiv:2312.11805*, 2023.
- Yuntao Bai, Saurav Kadavath, Sandipan Kundu, Amanda Askell, Jackson Kernion, Andy Jones, Anna Chen, Anna Goldie, Azalia Mirhoseini, Cameron McKinnon, et al. Constitutional ai: Harmlessness from ai feedback. *arXiv preprint arXiv:2212.08073*, 2022.
- Hugo Touvron, Thibaut Lavril, Gautier Izacard, Xavier Martinet, Marie-Anne Lachaux, Timothée Lacroix, Baptiste Rozière, Naman Goyal, Eric Hambro, Faisal Azhar, et al. Llama: Open and efficient foundation language models. *arXiv preprint arXiv:2302.13971*, 2023.
- Anju Rani, Daniel O Arroyo, and Petar Durdevic. Fungalzsl: A fine-grained synthetic dataset for zero-shot fungi classification. <https://data.mendeley.com/datasets/rw6ndgyrd7/1>, 2025a. Accessed: 2025-02-18.
- Anju Rani, Daniel O Arroyo, and Petar Durdevic. Synthetic fungi datasets: A time-aligned approach. *arXiv preprint arXiv:2501.02855*, 2025b.